



## Energy Harvesting from Vibrating Cantilever Structure of Different Base Materials using Piezoelectric Material: Theoretical and Experimental Approach

A. Krishna, S. Palanivelu\*

Vehicle Dynamics Laboratory, Department of Automotive Engineering, School of Mechanical Engineering, Vellore Institute of Technology, Vellore, India

### PAPER INFO

#### Paper history:

Received 14 June 2022

Received in revised form 27 October 2022

Accepted 03 November 2022

#### Keywords:

Piezoelectric Material

Frequency Spectrum Analysis

Energy Harvesting

### ABSTRACT

Energy conversion from one form to the other forms the basis for many inventions. Non utilized energy of mechanical vibration has attracted many researchers to focus on energy harvesting from vibrating structures. Piezoelectric material when attached to a vibrating structure converts mechanical energy into electrical energy. Today, harvesting energy ranges from micro level to macro level and has obtained its importance in wide range of real time application such as from low powered electronic devices to solar, wind and hydroelectric energy systems, respectively. The current work presents a detailed theoretical and experimental study on a cantilever type beam structure embedded with piezoelectric material on different base materials to understand micro level energy harvesting. Euler Bernoulli beam theory based mathematical model is excited with an impulse load at the free end for a broader frequency spectrum analysis. Finally, the proposed energy harvesters, cantilever specimens of three different base materials are ranked based on their maximum voltage and maximum instantaneous power outputs experimentally for the given impulse excitation. Out of three base materials considered steel and copper-based energy harvesters generated a maximum voltage output of 0.16mV and 0.13mV, respectively which corresponds to a maximum instantaneous power output of approximately 1.96nW and 1.69nW, respectively. Aluminum-based energy harvester performed the least among the three contributing to 0.81nW.

doi: 10.5829/ije.2023.36.01a.17

### NOMENCLATURE

$\omega$	Angular natural frequency		
$A(x)$	Area	$h_b$	Height of the base layer
$YI$	Bending modulus	$h_p$	Height of the piezoelectric layer
$\varepsilon_1$	Axial strain	$L$	Length
$\sigma_1$	Bending stress	$R_L$	Load resistance
$B$	Breadth	$m$	Mass
$i(t)$	Current	$r$	Mode number
$\rho$	Density	$M(x, t)$	Moment function
$W(x, t)$	Displacement function	$\varepsilon_{33}^s$	Permittivity at constant strain
$T_r(t)$	Displacement function with 't' variable alone	$\varepsilon_{33}^T$	Permittivity at constant stress
$\varphi_r(x)$	Displacement function with the 'x' variable alone	$d_{31}$	Piezoelectric moduli
$x$	Distance	$V(x, t)$	Shear force function
$h_{pc}$	Distance between the neutral axis of layers	$C_s$	Strain rate damping coefficient
$q(t)$	Electric charge	$C_a$	Viscous air damping coefficient
$D$	Electric displacement vector	$t$	Time
$E$	Electric field	$v(t)$	Voltage
$f(x, t)$	Force function	$Y_b$	Young's modulus of the base material
$P_y$	Impulse Load	$Y_p$	Young's modulus of piezoelectric material

\*Corresponding Author Institutional Email: [psakthivel@vit.ac.in](mailto:psakthivel@vit.ac.in)  
(S. Palanivelu)

Please cite this article as: A. Krishna, S. Palanivelu, Energy Harvesting from Vibrating Cantilever Structure of Different Base Materials using Piezoelectric Material: Theoretical and Experimental Approach, *International Journal of Engineering, Transactions A: Basics*, Vol. 36, No. 01, (2023), 152-162

## 1. INTRODUCTION

Piezoelectric, magnetostrictive, electromagnetic and electrostatic are the most researched energy harvesting technologies from environmental vibration in recent years due to their appreciable advantages such as fewer constraints in utilization, accessibility and availability in abundance in nature. Among these methods, piezoelectric energy transduction procedure is highly reliable and popular for the following reasons; Bulky bias magnets and pickup coils, makes the Magnetostrictive transduction method highly nonlinear and complicated. Chae et al. [1] proposed a linear energy harvester based on the electromagnetic principle used in a combination of a sliding permanent magnetic array and a ferrofluid as a lubricant. Deng and Dapino [2] have published a review article on magnetostrictive vibration energy harvesters and their advantage over electrochemical batteries which requires frequent recharging. Due to the simplicity in implementation and high-reliability piezoelectric energy transduction devices are of great interest in recent years [3]. Lafarge et al. [3] presented their idea of harvesting energy using piezoelectric cantilever beams on a vehicle suspension with a validated simulation with prototype testing in the laboratory.

Today, we could witness there are many application areas, to mention a few, healthcare and lifestyle industries and automotive industries use extensively the application of wireless sensor networks such as electrocardiogram (ECG) patch, autonomous health monitoring systems, heart rate measurement sensors, tire pressure tracking system, assist technologies like antilock brake system (ABS) and traction control system (TCS), respectively. It requires uninterrupted power supply to sensors for their optimal performance. Vullers et al. [4] published their work on energy harvesting methods for such autonomous wireless sensor networks. Application of piezoelectric transducers bonded with the structure can be used for its health monitoring. One such application of piezoelectric transducers is reported in the article published by Delebarre et al. [5] for aeronautical composite structures in their production line. Another novelty in using piezoelectric materials in the automotive tire application is the direct conversion of energy obtained due to strain into electrical energy and the work carried out by Van Den Ende et al. [6] is an evidence for the same. Piezoelectric transducers can be accounted for harvesting energy from pneumatic tires due to the deflection it produces during loading. Khameneifar and Arzanpour [7] used stacked piezoelectric material inside the pneumatic tire structure to harvest energy from its vibration. The work carried out by Chan [8] emphasizes the application of piezoelectric energy harvesting method from bus vibration in the low frequency range up to 14

Hz to the tune of 90  $\mu$ W.

Geometrical aspects are very important for energy harvester. The work of Wu et al. [9] on an asymmetric type M-shaped cantilever with three proof masses at the end, a longitudinal zigzag structure proposed by Zhou et al. [10] enhances energy harvesting from low frequency vibration. A power peak of 330 $\mu$ W was observed at a resonant frequency of 16 Hz was reported by Zhao et al. [11] with an elastic thin beam of spiral shape model. Muthlif and Nordin [12] studied the effect of varying the dimensions of the piezoelectric cantilever beam from the voltage generation. Erturk et al. [13] reported a model consists of electromechanical elements with an L-shaped structure of a vertical and a horizontal thin beam, with lumped masses so that the conventional cantilever beams have almost similar resonant frequencies. A power of 0.65mW was produced at a frequency of 1.71 kHz over the resistance 5.6k $\Omega$  at 80 N force by a 25mm diameter piezoelectric membrane was reported by Ericka et al. [14] from an unimorph membrane. Tadi Beni et al. [15, 16] investigated with the help of nonlinear formulation of isotropic piezoelectric Euler-Bernoulli nano-beam formed the basis for low energy harvesting at nanolevel. Fakharian [17], designed a planar monopole antenna, a lowprofile structure with a fractal geometry based thin radiation patch material, that can operate at 10-dB impedance bandwidth from 0.92 to 2.58 GHz.

A state of the art review papers published by Wei and Jing [18], Dixit et al. [19] and Mahidur et al. [20] on various energy harvesting techniques and their wide range of viable applications is very interesting to read and comprehend our understanding of the topic well. Roundy and Wright [21] developed a power generating MEMS device with a thin-film piezoelectric material that offered a high power density. The cantilever model is fitted with a bimorph structure having proof mass added to its end to reduce its resonant frequency. It was found that a model of 170 $\times$ 260  $\mu$ m size generated 1  $\mu$ W of uninterrupted electrical power. Erturk and Inman [22] concluded based on their analytical study, a design that would generate a power of up to 250  $\mu$ W/cm<sup>3</sup> upon an excitation frequency of 120 Hz at 2.5 m/s<sup>2</sup>. Jia et al. [23] proposed a piezoelectric material based bimorph structure with more degrees of freedom model that improved energy harvester bandwidth from 6 Hz to 24 Hz. Shams Nateri and Azizollah Ganji [24] studied the effect of piezoelectric material properties on MEMS based hydrophone.

This paper presents micro level energy harvesting from a cantilever beam with three different base material when they are embedded with piezoelectric material through a detailed analytical formulation based on Euler Bernoulli beam theory with complementary finite element modal analysis and appropriate experimental study.

**2. MATHEMATICAL MODELING**

**2. 1. Euler Bernoulli Beam**

An unimorph cantilever shaped piezoelectric energy harvester is illustrated in Figure 1. Similar formulation can be observed from the paper published by Muthlif and Nordin [12] and Shah-Mohammadi et al. [25] to model a cantilever beam for energy harvesting study. A perfect bond is assumed to exist between the non-active and the active layers of the unimorph beam. The breadth of the beam is  $b$  in the Y-Z plane. The model is assumed to have a uniform cross-section and remains normal to the axis of deformation after deformation.

Also, strain rate (internal) and air (external) around the structure constitute the damping mechanism to account damping properties of the model. An impulse excitation  $P_y$  is given at the free end of the beam at time  $t=0$  s as shown in Figure 1. The electromechanically coupled equation obtained for the beam responses is solved using the separation of variables. The decoupled solution for the electrical and mechanical responses is determined using MATLAB.

In this section, the basic governing equation is formulated for an Euler Bernoulli Beam from the basic force balance and moment balance equations. A small section of elemental length ' $dx$ ' as revealed in Figure 2 taken at a distance ' $x$ ' from the fixed end. Figure 3 shows the free body diagram of the element, to represent the shear force and bending moment acting on the element that is taken for developing the mathematical differential equations and later integrated to the entire length with cross section shown in Figure 4 to obtain the general equation for the transverse displacement of the composite beam.

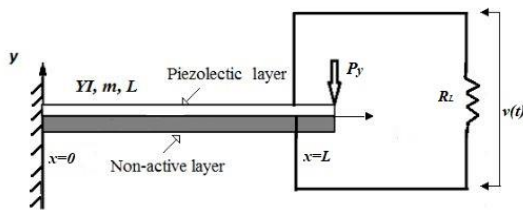


**Figure 1.** Piezoelectric energy harvester cantilever model

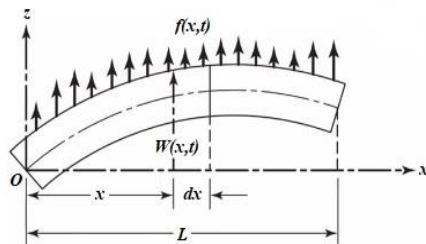


**Figure 2.** Euler Bernoulli Beam

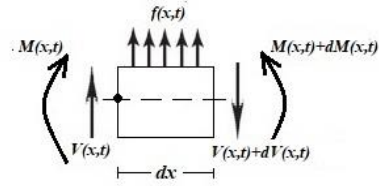


**Figure 3.** Cut section of Euler Bernoulli Beam

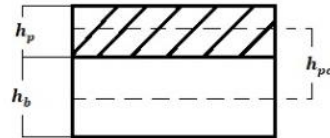


**Figure 4.** Cross-sectional view of the cantilever beam

Force equation:

$$\rho[A(x)]dx \frac{\partial^2 w(x,t)}{\partial t^2} = V - (V + dV) + f(x,t)dx \tag{1}$$

Moment equation:

$$(M + dM) - M - ((V + dV)dx) + f(x,t)dx \frac{dx}{2} = 0 \tag{2}$$

$$dV = \frac{\partial V}{\partial x} dx \tag{3}$$

$$dM = \frac{\partial M}{\partial x} dx \tag{4}$$

Substituting Equation (3) into Equation (1) leads to,

$$\rho A(x)dx \frac{\partial^2 w(x,t)}{\partial t^2} = -\frac{\partial V}{\partial x} dx + f(x,t)dx \tag{5}$$

Substituting Equations (3) and (4) in Equation (2) leads to:

$$\frac{\partial M}{\partial x} dx - Vdx - \frac{\partial V}{\partial x} dx^2 + f(x,t) \frac{dx^2}{2} = 0 \tag{6}$$

The term  $dx^2$  can be approximated to 0 (negligible value), therefore:

$$V = \frac{\partial M(x,t)}{\partial x} \tag{7}$$

Substituting Equation (7) into Equation (5):

$$\rho A \frac{\partial^2 w(x,t)}{\partial t^2} = -\frac{\partial^2 M(x,t)}{\partial x^2} + f(x,t) \tag{8}$$

According to Euler-Bernoulli beam theory:

$$M(x,t) = YI(x) \frac{\partial^2 w(x,t)}{\partial x^2} \tag{9}$$

Substituting Equation (9) into Equation (8) and thus Equation (8) can be rewritten as:

$$\rho A(x) \frac{\partial^2 w(x,t)}{\partial t^2} = -\frac{\partial^2}{\partial x^2} \left( YI(x) \frac{\partial^2 w(x,t)}{\partial x^2} \right) + f(x,t) \tag{10}$$

For a uniform beam, the geometric or material properties do not change along the x-direction. Thus:

$$\rho A \frac{\partial^2 W(x,t)}{\partial t^2} + YI \frac{\partial^4 W(x,t)}{\partial x^4} = f(x, t) \quad (11)$$

Equation (11) is the general equation for the transverse displacement of the beam.

## 2. 2. Mechanical Equation of Motion with Electrical Coupling

Incorporating the two types of damping mechanisms, one the viscous damping for air and the other is Kelvin-Voigt damping for strain rate to account bending from both spring and the dashpot, into the general Equation (11). This model is widely used to account creep phenomenon due to viscoelastic nature of the material in Euler-Bernouli beam and more about this constitute model can be observed from literature [26, 27]. Thus, according to the effect of base excitation, the general equation of motion can be written as follows:

$$\frac{\partial^2 M(x,t)}{\partial x^2} + C_s I \frac{\partial^2 W(x,t)}{\partial x^2 \partial t} + C_a \frac{\partial W(x,t)}{\partial t} + m \frac{\partial^2 W(x,t)}{\partial t^2} = f(x, t) \quad (12)$$

The stress-strain relationship of the beam and the piezoelectric (PZT) layer is given by Equation (13),

$$\sigma_1^b = Y_b \varepsilon_1^b \quad (13)$$

$$\sigma_1^p = Y_p (\varepsilon_1^p - d_{31} E_3) \quad (14)$$

Subscripts 1, 3 in Equation (14) refer to  $x$  and  $y$  directions respectively, and denote axial strain and polarization directions. The first moment of stress distribution across the cross-section is integrated to get internal moment.

$$M(x, t) = - \int_{-(h_b/2)}^{(h_b/2)} \sigma_1^b y dy - \int_{(h_b/2)}^{(h_b/2)+h_p} \sigma_1^p y dy \quad (15)$$

Since the cantilever beam comprises of both base material and PZT material, the terms  $m$ , and  $YI$  should be expressed for the composite beam.

$$m = B(\rho_b h_b + \rho_p h_p) \quad (16)$$

$$YI = B \left[ Y_b \left( \frac{h_b^3}{12} \right) + \frac{Y_p}{3} \left( \left( \frac{h_p}{2} + h_p \right)^3 - \left( \frac{h_b^3}{8} \right) \right) \right] \quad (17)$$

The strain due to bending is obtained in terms of the radius of curvature.

$$\varepsilon_1 = -y \frac{\partial^2 W(x,t)}{\partial x^2} \quad (18)$$

Using Equations (13), (14) and (18), the internal moment equation can be modified to:

$$M(x, t) = YI \frac{\partial^2 W(x,t)}{\partial x^2} + \vartheta v(t) \quad (19)$$

where,

$$\vartheta = - \frac{Y_p B d_{31}}{2} (h_p + h_b) \quad (20)$$

If the active piezoelectric layer does not cover the entire length of the beam but to a distance ' $x$ ' where  $x < L$ , then the coupling term  $\vartheta$  needs to be multiplied by the Heaviside function.

Equation (19) can be re-written as:

$$M(x, t) = YI \frac{\partial^2 W(x,t)}{\partial x^2} + \vartheta v(t) [H(x) - H(x - L)] \quad (21)$$

With Equation (21), we can rewrite Equation (11) as:

$$YI \frac{\partial^4 W(x,t)}{\partial x^4} + C_s I \frac{\partial^5 W(x,t)}{\partial x^4 \partial t} + C_a \frac{\partial W(x,t)}{\partial t} + m \frac{\partial^2 W(x,t)}{\partial t^2} + \vartheta v(t) \left[ \frac{d\delta(x)}{dx} - \frac{d\delta(x-L)}{dx} \right] = -P_y \delta(x - L) \delta(t) \quad (22)$$

where,  $(-P_y \delta(x - L) \delta(t))$  is an impulse excitation given at the free end of the beam at  $t=0$  s. Equation (22) is the mechanical governing Equation of motion with electric coupling shown in Figure 5.  $C_p$  represents the capacitance of the piezoelectric material, and  $R_L$  denotes the internal loss and the circuit is used for converting the mechanical stress into current.

## 2. 3. General Solution

Equation (22) is solved considering position and time dependency parts of displacement using principle of separation of variables and the solution is given by Equation (23):

$$W(x, t) = \sum_{r=1}^{\infty} \varphi_r(x) T_r(t) \quad (23)$$

where,  $\varphi_r(x)$  refer to mass normalized eigen functions and  $T_r(t)$  refer to the modal coordinates of the beam considered for its  $r^{\text{th}}$  mode. For proportionately damped system the eigenfunction denoted by  $\varphi_r(x)$  is the same as the eigenfunction for an undamped beam undergoing free vibration.

$$\varphi_r(x) = \sin \left( \frac{\beta_r x}{L} \right) - \sinh \left( \frac{\beta_r x}{L} \right) + \lambda_r \left[ \cos \left( \frac{\beta_r x}{L} \right) - \cosh \left( \frac{\beta_r x}{L} \right) \right] \quad (24)$$

$\beta_r$  represents a range of frequency numbers of its dimensionless form and obtained by solving the characteristic Equation given by Equation (25):

$$1 + \cos \beta_r \cosh \beta_r = 0 \quad (25)$$

and:

$$\lambda_r = \frac{-\cos \beta_r - \cosh \beta_r}{-\sin \beta_r + \sinh \beta_r} \quad (26)$$

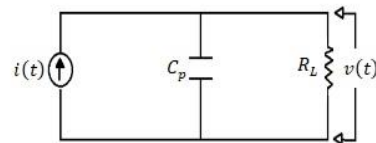


Figure 5. Simple Electrical circuit for the energy harvester

The roots of Equation (25) are obtained by using a MATLAB function 'fzero'. The first 4 values of  $\beta_r$  are  $\beta_1 = \pm 1.875$ ;  $\beta_2 = \pm 4.694$ ;  $\beta_3 = \pm 7.8547$ ; and  $\beta_4 = \pm 10.9955$ ; hence,  $\beta_r \approx (2r - 1)\frac{\pi}{2}$  with all  $r \geq 3$

The mass normalized eigenfunction  $\varphi_r(x)$  must satisfy the orthogonality condition given by Equation (27):

$$\int_{x=0}^L m \varphi_s \varphi_r dx = \delta_{rs} \quad (27)$$

The undamped natural frequency  $\omega_r$  is expressed as:

$$\omega_r = \beta_r^2 \sqrt{\frac{YI}{\rho A}} \quad (28)$$

Equation (22) is multiplied by  $\varphi_s$  and integrated between 0 to L to get the coupled electromechanical differential equation to solve for the modal response and is given by Equation (29):

$$\frac{\partial^2 T(t)}{\partial t^2} + 2\xi_r \omega_r \frac{\partial T(t)}{\partial t} + \omega_r^2 T(t) + \chi_r v(t) = F_r(t) \quad (29)$$

where:

$$2\xi_r = \left( \frac{C_s I \omega_r}{2YI} + \frac{C_d}{2m\omega_r} \right) \quad (30)$$

$$\chi_r = \vartheta \left( \frac{d\varphi(x)}{dx} \right)_{x=L} \quad (31)$$

The mechanical damping as mentioned earlier the strain rate and viscous air-damping are given by  $2\xi_r$ . Equation (29) is solved using Duhamel's integral and is given by Equation (32):

$$T(t) = \frac{1}{\omega_{d_r}} \int_{\tau=0}^t [F_r(\tau) - \chi_r v(\tau)] e^{-\xi_r \omega_r (t-\tau)} \sin(\omega_{d_r} (t-\tau)) d\tau \quad (32)$$

where,  $\omega_{d_r} = \omega_r \sqrt{1 - \xi_r^2}$  is the damped natural frequency of the  $r^{\text{th}}$  mode.

**2. 4. Electrical Circuit Equation** The electrical circuit equation with mechanical coupling term is obtained by considering the following piezoelectric constitutive relation:

$$D_3 = d_{31} \sigma_1 + \varepsilon_{33}^T E_3 \quad (33)$$

Equation (33) is modified to express axial stress  $\sigma_1$  in terms of bending strain ( $\varepsilon_1$ ) and Young's modulus of piezoelectric material ( $Y_p$ ). Since  $\varepsilon_{33}^T = \varepsilon_{33}^S + d_{31}^2 Y_p$ , we replace permittivity at constant stress ( $\varepsilon_{33}^T$ ) with permittivity at constant strain ( $\varepsilon_{33}^S$ ). Also  $E(t) = -\frac{v(t)}{h_p}$ .

Therefore Equation (33) becomes:

$$D_3(x, t) = -d_{31} Y_p h_{pc} \frac{\partial^2 W(x, t)}{\partial x^2} - \varepsilon_{33}^S \frac{v(t)}{h_p} \quad (34)$$

where,  $h_{pc}$  is the distance from the neutral axis to the center of the piezoelectric layer of the beam considered. The electric charge  $q(t)$  generated can be obtained by integrating the electric displacement over the electrode area:

$$q(t) = \int D \cdot \hat{n} dA = - \int_{x=0}^L \left( d_{31} Y_p h_{pc} B \frac{\partial^2 W(x, t)}{\partial x^2} + \varepsilon_{33}^S B \frac{v(t)}{h_p} \right) dx \quad (35)$$

$$i(t) = \frac{dq(t)}{dt} = - \int_{x=0}^L \left( d_{31} Y_p h_{pc} B \frac{\partial^3 W(x, t)}{\partial x^2 \partial t} + \frac{\varepsilon_{33}^S B L}{h_p} \frac{dv(t)}{dt} \right) dx \quad (36)$$

$$v(t) = R_L i(t) = -R_L \left\{ \int_{x=0}^L \left( d_{31} Y_p h_{pc} B \frac{\partial^3 W(x, t)}{\partial x^2 \partial t} + \frac{\varepsilon_{33}^S B L}{h_p} \frac{dv(t)}{dt} \right) dx \right\} \quad (37)$$

Thus, the electric circuit equation can be written as:

$$\frac{\varepsilon_{33}^S B L}{h_p} \frac{dv(t)}{dt} + \frac{v(t)}{R_L} = - \int_{x=0}^L \left( d_{31} Y_p h_{pc} B \frac{\partial^3 W(x, t)}{\partial x^2 \partial t} \right) dx \quad (38)$$

Equation (39) is obtained from the circuit is shown in Figure 5 applying Kirchhoff's law.

$$C_p \frac{dv(t)}{dt} + \frac{v(t)}{\tau_c} = \sum_{r=1}^{\infty} \varphi_r \frac{dT_r(t)}{dt} \quad (39)$$

where,

$$\varphi_r = \frac{d_{31} Y_p h_{pc} h_p}{\varepsilon_{33}^S B L} \left( \frac{d\varphi_r(x)}{dx} \right)_{x=L} \quad (40)$$

$$\tau_c = \frac{R_L \varepsilon_{33}^S B L}{h_p} \quad (41)$$

Leibniz rule is used to carry out differentiation operation under an integral sign. Substituting  $\frac{dT}{dt}$  in the above equation leads to:

$$\frac{dv(t)}{dt} = \frac{d}{dt} \int_{\tau=0}^t [F_r(\tau) + \chi_r v(\tau)] e^{-\xi_r \omega_r (t-\tau)} \sin(\omega_{d_r} (t-\tau)) d\tau + \int_{\tau=0}^t [F_r(\tau) + \chi_r v(\tau)] e^{-\xi_r \omega_r (t-\tau)} (-\xi_r \omega_r \sin(\omega_{d_r} (t-\tau)) + \omega_{d_r} \cos(\omega_{d_r} (t-\tau))) d\tau \quad (42)$$

Therefore,

$$\frac{dv(t)}{dt} + \frac{v(t)}{\tau_c} = \sum_{r=1}^{\infty} \varphi_r \int_{\tau=0}^t [F_r(\tau) + \chi_r v(\tau)] e^{-\xi_r \omega_r (t-\tau)} (-\xi_r \omega_r \sin(\omega_{d_r} (t-\tau)) + \omega_{d_r} \cos(\omega_{d_r} (t-\tau))) d\tau \quad (43)$$

Equation (43) is solved using Laplace transforms and thus a decoupled solution for the voltage function  $v(t)$  is obtained. The right hand side of the equation is expressed by a convolution of two terms  $t$  and  $\tau$ , where in Laplace transform it can be defined as the product of Laplace transform of each term individually. A stepwise procedure is explained to apply Laplace transform and the final expression for voltage is shown below,

$$sV(s) + \frac{1}{\tau_c} V(s) = \sum_{r=1}^{\infty} \{ \varphi_r L[-P_y \delta(t)] + \chi_r v(t) L[e^{\xi_r \omega_r (t-\tau)} \sin \omega_d (t-\tau)] + \chi_r v(t) L[\omega_d \cos \omega_d (t-\tau)] \} \quad (44)$$

$$sV(s) + \frac{1}{\tau_c} V(s) = \sum_{r=1}^{\infty} \varphi_r [-P_y \varphi_{x=L} + \chi_r V(s)] \left( \frac{-\xi_r \omega_r \omega_d}{(s + \xi_r \omega_r)^2 + \omega_d^2} + \left( \frac{\omega_d (s + \xi_r \omega_r)}{(s + \xi_r \omega_r)^2 + \omega_d^2} \right) \right) \quad (45)$$

which implies,

$$V(s) = \frac{(-P_y \varphi_{x=L} \varphi_r \omega_d \tau_c \chi_r) s}{\tau_c s^3 + (2\xi_r \omega_r + 1) s^2 + (\tau_c \omega_r^2 + 2\xi_r \omega_r + \chi_r \varphi_r \omega_d \tau_c) s + \omega_r^2} \quad (46)$$

The values of  $\omega_r$ ,  $\omega_d$ ,  $\tau_c$ ,  $\chi_r$  can be obtained from the formulas expressed above. The first four modes were taken for analyzing the solution. The damping ratios considered are given in brackets (0.010, 0.013, 0.033, 0.064, 0.106) were experimentally calculated for the same dimensions reported in the literature [17]. Equation (46) becomes:

$$V(s) = (-P_y \varphi_{x=L} \varphi_r \omega_d \tau_c) \left( \frac{s}{(s-a)(s-b)(s-c)} \right) \quad (47)$$

Inverse Laplace transform applied on Equation (47) gives a closed form decoupled expression for voltage that is generated within the considered piezoelectric layer for impulse excitation given at the tip.

$$v(t) = (-P_y \varphi_{x=L} \varphi_r \omega_d \tau_c) (Ae^{at} + Be^{bt} + Ce^{ct}) \quad (48)$$

Where:

$$A = \frac{a}{(a-b)(a-c)}, B = \frac{b}{(a-b)(b-c)}, C = \frac{c}{(a-c)(b-c)} \quad (49)$$

Substituting  $v(t)$  in Equation (32) a decoupled solution is obtained for the modal response of the considered unimorph cantilever beam and upon integrating the expression from  $\tau = 0$  to  $t$ , the solution obtained can be written as:

$$\begin{aligned} T(t) = & -P_y \varphi_{x=L} e^{-\xi_r \omega_r t} \sin(\omega_d t) + \\ & \chi_r P_y \varphi_{x=L} \varphi_r \omega_d \tau_c \left[ \left( \frac{A}{(a+\xi_r \omega_r)^2 + \omega_d^2} (e^{at} + e^{-\xi_r \omega_r t} ((a + \xi_r \omega_r) \sin(\omega_d t) - \omega_d \cos(\omega_d t))) \right) + \left( \frac{B}{(b+\xi_r \omega_r)^2 + \omega_d^2} (e^{bt} + e^{-\xi_r \omega_r t} ((b + \xi_r \omega_r) \sin(\omega_d t) - \omega_d \cos(\omega_d t))) \right) + \left( \frac{C}{(c+\xi_r \omega_r)^2 + \omega_d^2} (e^{ct} + e^{-\xi_r \omega_r t} ((c + \xi_r \omega_r) \sin(\omega_d t) - \omega_d \cos(\omega_d t))) \right) \right] \end{aligned} \quad (50)$$

Therefore,  $W(x, t) = \sum_{r=1}^{\infty} \varphi_r(x) T_r(t)$  can be written as:

$$\begin{aligned} W(x, t) = & \sum_{r=1}^{\infty} \left\{ \sin - \sinh \left( \frac{\beta_r x}{L} \right) + \lambda_r \left[ \cos \left( \frac{\beta_r x}{L} \right) - \cosh \left( \frac{\beta_r x}{L} \right) \right] \right\} \left\{ -P_y \varphi_{x=L} e^{-\xi_r \omega_r t} \sin(\omega_d t) + \chi_r P_y \varphi_{x=L} \varphi_r \omega_d \tau_c \left[ \left( \frac{A}{(a+\xi_r \omega_r)^2 + \omega_d^2} (e^{at} + e^{-\xi_r \omega_r t} ((a + \xi_r \omega_r) \sin(\omega_d t) - \omega_d \cos(\omega_d t))) \right) + \left( \frac{B}{(b+\xi_r \omega_r)^2 + \omega_d^2} (e^{bt} + e^{-\xi_r \omega_r t} ((b + \xi_r \omega_r) \sin(\omega_d t) - \omega_d \cos(\omega_d t))) \right) + \left( \frac{C}{(c+\xi_r \omega_r)^2 + \omega_d^2} (e^{ct} + e^{-\xi_r \omega_r t} ((c + \xi_r \omega_r) \sin(\omega_d t) - \omega_d \cos(\omega_d t))) \right) \right] \right\} \end{aligned} \quad (51)$$

### 3. FINITE ELEMENT SIMULATION

A finite element cantilever shaped piezoelectric energy harvester with and without tip mass is modeled in ABAQUS for finite element modal analysis of the compound structure to understand its mechanical

behavior and to determine the fundamental natural frequency.

### 3. 1. Model Geometry and Material Definition

TABLE 1. Properties of the base material

Properties of material	Aluminum	Copper	Steel	Unit
Density	2800	8700	8000	kg/m <sup>3</sup>
Young's Modulus	70×10 <sup>9</sup>	110×10 <sup>9</sup>	215×10 <sup>9</sup>	N/m <sup>2</sup>
Poisson's Ratio	0.3	0.3	0.3	-

TABLE 2. Properties of Piezoelectric material

Parameters	PZT-5H	Unit
Density	7500	kg/m <sup>3</sup>
Uniaxial Modulus (E1)	60.61×10 <sup>9</sup>	N/m <sup>2</sup>
Uniaxial Modulus (E2)	60.61×10 <sup>9</sup>	N/m <sup>2</sup>
Uniaxial Modulus (E3)	48.31×10 <sup>9</sup>	N/m <sup>2</sup>
Poisson's Ratio (Nu12)	0.289	-
Poisson's Ratio (Nu13)	0.49	-
Poisson's Ratio (Nu23)	0.49	-
Shear Modulus (G12)	23.5×10 <sup>9</sup>	N/m <sup>2</sup>
Shear Modulus (G13)	23.0×10 <sup>9</sup>	N/m <sup>2</sup>
Shear Modulus (G23)	23.0×10 <sup>9</sup>	N/m <sup>2</sup>

The piezoelectric energy harvester is modeled as a cantilever beam of 100 mm length and 20 mm breadth. The thickness of the base material is 0.5 mm whereas that of the piezoelectric material is 0.4 mm. Three different base materials are used namely aluminum, copper and steel. Also, tip mass of 10 grams is attached to the free end of the cantilever beam to study its effect on the eigen frequencies. The properties of the base material, as well as the piezoelectric patch are shown in Tables 1 and 2, respectively.

### 3. 2. Assembly and Meshing

Meshing of the energy harvester model is done with 8 elements along with the thickness and mesh size of 0.001 along the width and length of the beam. SC8R element type which is a general purpose in-plane 8-noded quadrilateral continuum shell element, is selected for base material. PZT material has meshed with an approximate global size of 0.001. C3D8E element type which is an 8-node linear piezoelectric brick is assigned to the PZT patch. PZT patch and the base material are connected using tie constraints with node to surface discretization method.

The PZT patch is set to be the master surface while the base material is the slave surface.

**3. 3. Boundary Condition and Loading** All translational and rotational degrees of freedom are fixed at one end of the energy harvester. The modal analysis technique is carried out to determine the modal parameters of the cantilever shaped energy harvester. The effect of tip mass was well understood by adding a mass of 10 grams at the free end of the cantilever. The tip mass showed a progressive improvement in the overall design of the cantilever by lowering the eigen frequencies of the structure.

**4. EXPERIMENTAL ANALYSIS**

Figure 6 shows the experimental setup arranged to realize the proposed energy harvester. Energy harvester samples with three different base materials are used in this experiment. Samples are made with 3 PZT materials connected in series which are fixed on the respective base materials. The samples are clamped with a fixed base for support. An impulse load is applied using an impact hammer to understand the mechanical and electrical behavior of the system. An ICP type 100 mV/g sensitivity tri-axial accelerometer is attached to the cantilever obtains the vibration response of the structure. A clean, noise-free frequency response low cost PZT ceramic material of high dielectric constant value with high charge sensitivity is used. BNC cables are used to connect the accelerometer sensor as well as the PZT leads to the Dynamic Signal Analyzer (DSA). Impact hammer, PZT beam, and the accelerometer are connected to three different channels on the DSA which enables us to extract the required transfer function. Each sample is investigated for an average of 5 trials for accuracy. The spectral frequency range was limited to 100 Hz because the first mode lies within this range and it is at this initial mode that the energy harvester will be able to generate maximum output as all the other modes may result in the

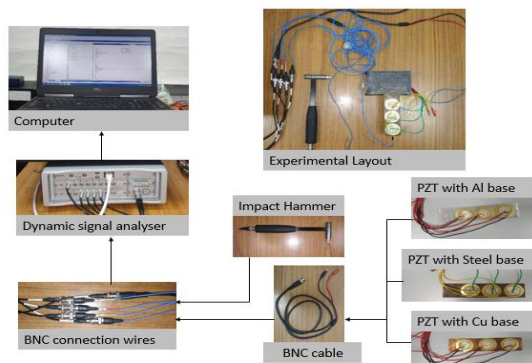


Figure 6. Experimental setup and the energy harvester

partial charge canceling due to opposite directional stress regions [23].

**5. RESULTS AND DISCUSSIONS**

**5. 1. Mathematical Modeling Results** Equation (24) is solved in MATLAB and is used to predict the mechanical behavior of the energy harvester corresponding to each mode as depicted in Figure 7. The derived Equations (48) and (51) represent the voltage and mechanical response respectively of the energy harvester under impulse loading. The equations are solved using MATLAB and the responses are studied for three different base materials such as aluminium, copper, and steel.

The time response of tip displacement and its frequency spectrum for aluminum base material are shown in Figures 8(a) and 8(b). A peak response at the time of impact decreases exponentially to zero value in a very short time interval. The frequency spectrum energy voltage function has its maximum amplitude at the first natural frequency of 52 Hz approximately and it is at this frequency that the harvester can produce maximum voltage amplitude of about 0.09 mV which is equivalent to an instantaneous power output of around  $0.81 \times 10^{-9} \text{W}$  across a  $10 \Omega$  load resistance.

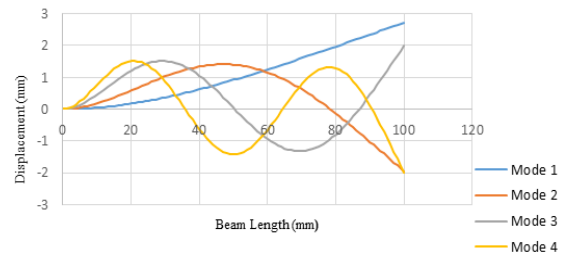
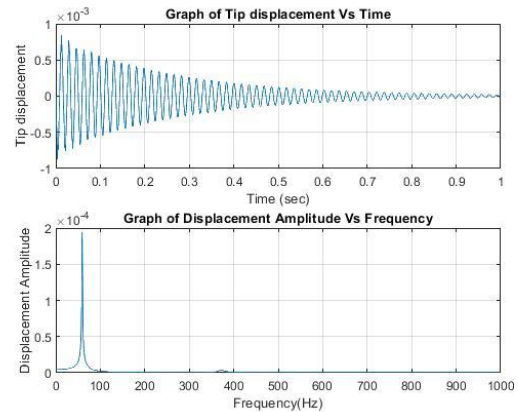
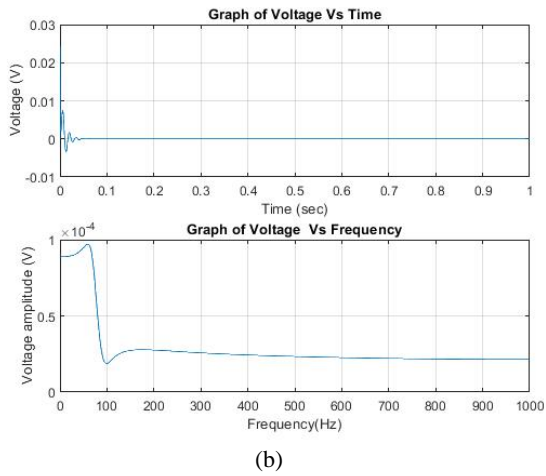


Figure 7. Mode shapes of the proposed rectangular cantilever beam



(a)



**Figure 8.** (a) Graph of tip displacement as function of time and its corresponding frequency spectrum, (b) Graph of voltage response as a function of time and its corresponding frequency spectrum for Aluminium

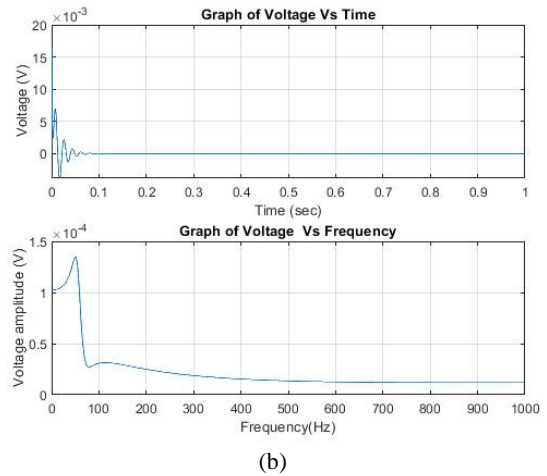


**Figure 9.** (a) Graph of tip displacement as function of time and its corresponding frequency spectrum, (b) Graph of voltage response as a function of time and its corresponding frequency spectrum for Copper

A similar trend in tip displacement and voltage generated can be seen in copper and steel-based harvesters. Figures 9(a) and 9(b) and Figures 10(a) and 10(b) show the variation of tip displacement and voltage as time varies and its frequency spectrum for copper and steel respectively.

The copper-based energy harvester was capable of generating an output voltage of 0.13 mV while that of steel showed the highest voltage reading of approximately 0.14 mV. Steel-based energy harvester showed a slightly better energy harvesting capability among the three base elements. The average instantaneous power output of copper and steel across a load resistance of  $10\Omega$  comes out to be around  $1.69 \times 10^{-9}$  W and  $1.96 \times 10^{-9}$  W, respectively. Even though a small peak is seen in the frequency range of 200 Hz to 300 Hz where the second natural frequency of the harvester lie,

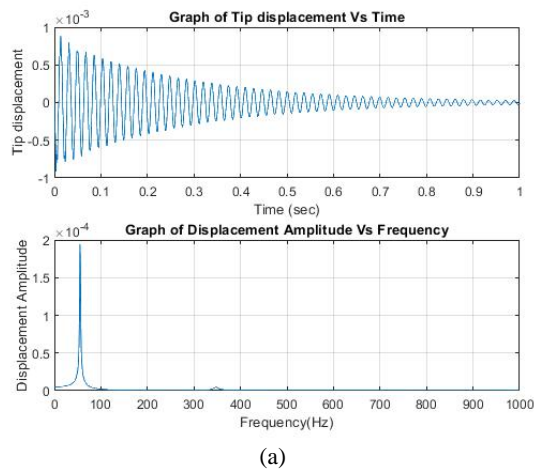


**Figure 10.** (a) Graph of tip displacement as function of time and its corresponding frequency spectrum, (b) Graph of voltage response as a function of time and its corresponding frequency spectrum for Steel

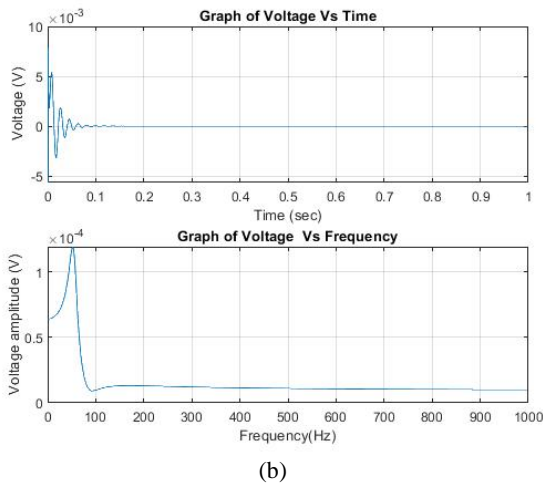
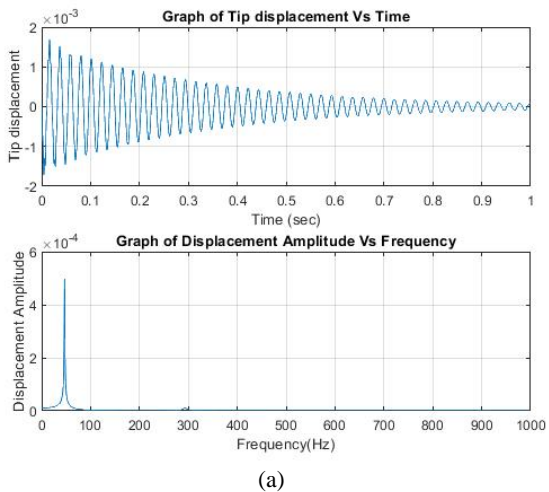


**Figure 10.** (a) Graph of tip displacement as function of time and its corresponding frequency spectrum, (b) Graph of voltage response as a function of time and its corresponding frequency spectrum for Steel

it is not taken into consideration as the energy harvested at the first natural frequency has the highest magnitude. A similar observation can be ascribed from literature [7].

**5. 2. Modal Analysis Results** Figures 11 and 12 depict the first four mode shapes of the proposed cantilever shaped energy harvester without tip mass and with tip mass (10 g), respectively. Furthermore, the addition of tip mass drastically lowers the natural frequency of the cantilever beam as mentioned in Table 3. However, the whole study is restricted to the first natural frequency because only this region yields maximum voltage output [23]. Hence it is proposed to examine the frequency response function obtained for the impulse excitation where accelerometer mass act as the tip mass.

**5. 3. Experimental Results** Figure 13 deals with the electrical and mechanical responses of the three samples to time. An exponential decay can be observed over both the responses for not more than one second. These trends are validated with similar observations from mathematical modeling depicted in the previous section.

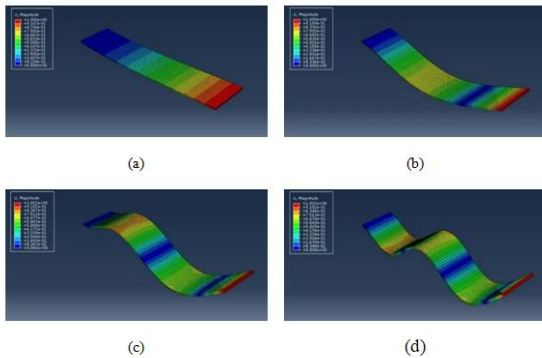


**Figure 11.** Different mode shapes of simple cantilever shaped energy harvester without tip mass: (a) 1<sup>st</sup> Mode, (b) 2<sup>nd</sup> Mode, (c) 3<sup>rd</sup> Mode, (d) 4<sup>th</sup> Mode

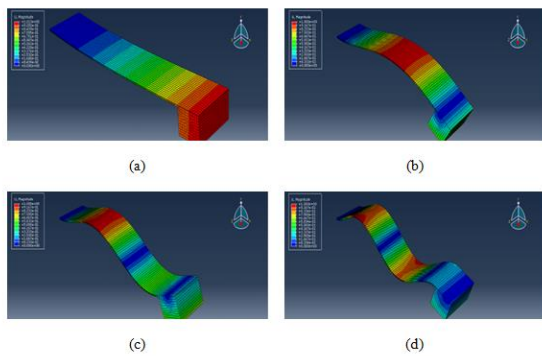


**Figure 12.** Different mode shapes of simple cantilever shaped energy harvester with tip mass: (a) 1<sup>st</sup> Mode, (b) 2<sup>nd</sup> Mode, (c) 3<sup>rd</sup> Mode, (d) 4<sup>th</sup> Mode

**TABLE 3.** Reduction in natural frequencies due to the addition of tip mass

Mode number	Natural Frequency (Hz)					
	Copper		Steel		Aluminum	
	0 gm	10 gm	0 gm	10 gm	0 gm	10 gm
1	41.014	16.48	49.863	16.078	44.642	30.343
2	257.08	237.06	312.5	126.07	279.85	278
3	410.28	257.09	477.95	175.33	477.19	310.39
4	721.03	644.81	876.2	483.68	784.78	801.37

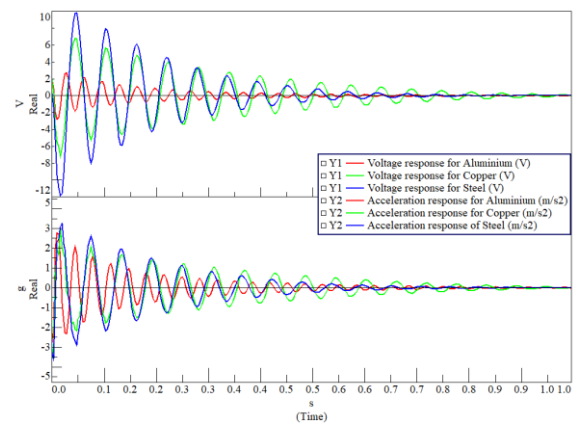


**Figure 13.** Voltage and acceleration response for three samples as a function of time

The corresponding frequency spectra are depicted in Figure 14 where the frequency of interest is restricted to 100 Hz because maximum energy harvesting is occurring at a first natural frequency according to literature [21].

The result indicates that steel and copper-based energy harvesters were capable of generating an instantaneous voltage output of 0.13mV and 0.11mV, respectively while aluminum-based energy harvester was

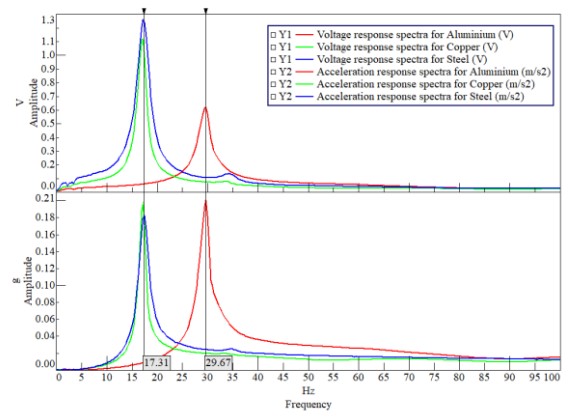


**Figure 14.** Voltage and acceleration response for three samples as a function of frequency

capable of generating a mere 0.06mV at its first natural frequency. Importantly, the effect of tip mass is captured during the experiment and it almost closer to the numerical results frequencies given in Table 3 for different base material with tip mass.

## 6. CONCLUSION

This paper distinctively investigates the energy harvesting capability for a given impulse loading condition that characterizes our test specimen's energy transfer characteristics. The finite element modal analysis results showed a detrimental reduction in the natural frequency of the cantilever structure upon the addition of a tip mass. The first natural frequency of Copper and Steel reduced to 16.48 Hz and 16.078 Hz, respectively; while that of Aluminum dropped down to 30.343 Hz with the addition of 10gm tip mass. Experimental work carried out exposes the wide range of possibilities as well as simplicity in using piezoelectric material in vibration energy harvesting. Among the three base materials mentioned in this work, steel and copper-based energy harvesters were capable of generating a maximum voltage output of 0.16mV and 0.13mV, respectively which corresponds to a maximum instantaneous power output of approximately 1.96nW and 1.69nW, respectively. However, aluminum-based energy harvester performed the least among the three contributing to a mere 0.81nW.

## 7. ACKNOWLEDGMENT

Authors convey their sincere thanks to Vehicle Dynamics Laboratory, Department of Automotive Engineering, Vellore Institute of Technology, Vellore for the test facility provided to carry out the necessary experiments for the current paper.

## 8. REFERENCES

- Chae, S.H., Ju, S., Choi, Y., Chi, Y.-E. and Ji, C.-H., "Electromagnetic linear vibration energy harvester using sliding permanent magnet array and ferrofluid as a lubricant", *Micromachines*, Vol. 8, No. 10, (2017), 288. <https://doi.org/10.3390/mi8100288>
- Deng, Z. and Dapino, M.J., "Review of magnetostrictive vibration energy harvesters", *Smart Materials and Structures*, Vol. 26, No. 10, (2017), 103001.
- Lafarge, B., Grondel, S., Delebarre, C. and Cattan, E., "A validated simulation of energy harvesting with piezoelectric cantilever beams on a vehicle suspension using bond graph approach", *Mechatronics*, Vol. 53, (2018), 202-214. <https://doi.org/10.1016/j.mechatronics.2018.06.004>
- Vullers, R.J., Van Schaijk, R., Visser, H.J., Penders, J. and Van Hoof, C., "Energy harvesting for autonomous wireless sensor networks", *IEEE Solid-State Circuits Magazine*, Vol. 2, No. 2, (2010), 29-38. doi: 10.1109/MSSC.2010.936667.
- Delebarre, C., Grondel, S. and Rivart, F., "Autonomous piezoelectric structural health monitoring system for on-production line use", *Advances in Applied Ceramics*, Vol. 114, No. 4, (2015), 205-210. <https://doi.org/10.1179/1743676114Y.0000000220>
- Van den Ende, D., Van de Wiel, H., Groen, W. and Van der Zwaag, S., "Direct strain energy harvesting in automobile tires using piezoelectric pzt-polymer composites", *Smart Materials and Structures*, Vol. 21, No. 1, (2011), 015011.
- Khameneifar, F. and Arzanpour, S., "Energy harvesting from pneumatic tires using piezoelectric transducers", in *Smart Materials, Adaptive Structures and Intelligent Systems*. Vol. 43314, (2008), 331-337.
- Chan, M., "Low-grade waste vibration energy recovery from hong kong franchised buses", *International Journal of Green Energy*, Vol. 11, No. 4, (2014), 431-437. <https://doi.org/10.1080/15435075.2013.777913>
- Wu, M., Ou, Y., Mao, H., Li, Z., Liu, R., Ming, A. and Ou, W., "Multi-resonant wideband energy harvester based on a folded asymmetric m-shaped cantilever", *Aip Advances*, Vol. 5, No. 7, (2015), 077149. <https://doi.org/10.1063/1.4927466>
- Zhou, S., Chen, W., Malakooti, M.H., Cao, J. and Inman, D.J., "Design and modeling of a flexible longitudinal zigzag structure for enhanced vibration energy harvesting", *Journal of Intelligent Material Systems and Structures*, Vol. 28, No. 3, (2017), 367-380. doi: <https://doi.org/10.1177/1045389X16645862>
- Zhao, N., Yang, J., Yu, Q., Zhao, J., Liu, J., Wen, Y. and Li, P., "Three-dimensional piezoelectric vibration energy harvester using spiral-shaped beam with triple operating frequencies", *Review of Scientific Instruments*, Vol. 87, No. 1, (2016), 015003. <https://doi.org/10.1063/1.4940417>
- Muthalif, A.G. and Nordin, N.D., "Optimal piezoelectric beam shape for single and broadband vibration energy harvesting: Modeling, simulation and experimental results", *Mechanical Systems and Signal Processing*, Vol. 54, (2015), 417-426. <https://doi.org/10.1016/j.ymsp.2014.07.014>
- Erturk, A., Renno, J.M. and Inman, D.J., "Modeling of piezoelectric energy harvesting from an l-shaped beam-mass structure with an application to uavs", *Journal of Intelligent Material Systems and Structures*, Vol. 20, No. 5, (2009), 529-544. <https://doi.org/10.1177/1045389X08098096>
- Ericka, M., Vasic, D., Costa, F., Poulin, G. and Tliba, S., "Energy harvesting from vibration using a piezoelectric membrane", in *Journal de Physique IV (Proceedings)*, EDP sciences. Vol. 128, (2005), 187-193.
- Y., T.B., A., J. and H., R., "Size effect on free transverse vibration of cracked nano-beams using couple stress theory", *International Journal of Engineering, Transactions B: Applications*, Vol. 28, No. 2, (2015), 296-304. doi: 10.5829/idosi.ije.2015.28.02b.17.
- Beni, Z.T., Ravandi, S.A.H. and Beni, Y.T., "Size effect on free transverse vibration of cracked nano-beams using couple stress theory", *International Journal of Engineering, Transactions C: Aspects*, Vol. 28, No. 2, (2015), 296-304. doi: 10.5829/ije.2018.31.09c.15.
- Fakharian, M., "A wideband fractal planar monopole antenna with a thin slot on radiating stub for radio frequency energy harvesting applications", *International Journal of Engineering, Transactions B: Applications*, Vol. 33, No. 11, (2020), 2181-2187. doi: 10.5829/ije.2020.33.11b.08.
- Wei, C. and Jing, X., "A comprehensive review on vibration energy harvesting: Modelling and realization", *Renewable and Sustainable Energy Reviews*, Vol. 74, (2017), 1-18. <https://doi.org/10.1016/j.rser.2017.01.073>

19. Dixit, N.K., K. J. Rangra and Y. C. Sharma, "Review study on piezoelectric energy harvesters and their applications", *International Journal of Computer Science Engineering*, Vol. 6, No. 9, (2018), 607-616. <https://doi.org/10.1016/j.joule.2018.03.011>
20. Sarker, M.R., Julai, S., Sabri, M.F.M., Said, S.M., Islam, M.M. and Tahir, M., "Review of piezoelectric energy harvesting system and application of optimization techniques to enhance the performance of the harvesting system", *Sensors and Actuators A: Physical*, Vol. 300, (2019), 111634. <https://doi.org/10.1016/j.sna.2019.111634>
21. Roundy, S. and Wright, P.K., "A piezoelectric vibration based generator for wireless electronics", *Smart Materials and Structures*, Vol. 13, No. 5, (2004), 1131.
22. Erturk, A. and Inman, D.J., "On mechanical modeling of cantilevered piezoelectric vibration energy harvesters", *Journal of Intelligent Material Systems and Structures*, Vol. 19, No. 11, (2008), 1311-1325. <https://doi.org/10.1177/1045389X07085639>
23. Jia, Y., Wei, X., Xu, L., Wang, C., Lian, P., Xue, S., Al-Saadi, A. and Shi, Y., "Multiphysics vibration fe model of piezoelectric macro fibre composite on carbon fibre composite structures", *Composites Part B: Engineering*, Vol. 161, (2019), 376-385. <https://doi.org/10.1016/j.compositesb.2018.12.081>
24. Shams Nateri, M. and Azizollah Ganji, B., "The effect of material properties on sensitivity of the microelectromechanical systems piezoelectric hydrophone", *International Journal of Engineering, Transactions C: Aspects*, Vol. 30, No. 12, (2017), 1848-1855. doi: 10.5829/ije.2017.30.12c.05.
25. Rezazadeh, G., Khanchehgardan, A., Shah-Mohammadi-Azar, A. and Shabani, R., "Mechanical response of a piezoelectrically sandwiched nano-beam based on the non-local theory", *International Journal of Engineering, Transactions C: Aspects*, Vol. 26, No. 12, (2013), 1515-1524. doi: 10.5829/idosi.ije.2013.26.12c.12.
26. Raposo, C., Bastos, W. and Avila, J., "A transmission problem for euler-bernoulli beam with kelvin-voigt damping", *Applied Mathematics and Information Sciences*, Vol. 5, No. 1, (2011), 17-28.
27. Hosseini Hashemi, S. and Bakhshi Khaniki, H., "Free vibration analysis of nonuniform microbeams based on modified couple stress theory: An analytical solution", *International Journal of Engineering, Transactions B: Applications*, Vol. 30, No. 2, (2017), 311-320. doi: 10.5829/idosi.ije.2017.30.02b.19.

---

### Persian Abstract

#### چکیده

تبدیل انرژی از یک شکل به شکل دیگر اساس بسیاری از اختراعات را تشکیل می دهد. انرژی استفاده نشده ارتعاش مکانیکی بسیاری از محققان را به تمرکز بر برداشت انرژی از سازه های ارتعاشی جذب کرده است. مواد پیزوالکتریک هنگامی که به یک ساختار ارتعاشی متصل می شوند، انرژی مکانیکی را به انرژی الکتریکی تبدیل می کنند. امروزه برداشت انرژی از سطح خرد تا سطح کلان متغیر است و اهمیت خود را در گستره وسیعی از کاربردهای بلادرنگ مانند از دستگاه های الکترونیکی کم توان گرفته تا سیستم های انرژی خورشیدی، بادی و برق آبی به دست آورده است. کار فعلی یک مطالعه تئوری و تجربی دقیق بر روی یک ساختار تیر از نوع کنسول تعبیه شده با مواد پیزوالکتریک بر روی مواد پایه مختلف برای درک میزان برداشت انرژی در سطح میکرو ارائه می کند. مدل ریاضی مبتنی بر تئوری پرتو اویلر برنولی با یک بار ضربه ای در انتهای آزاد برای تجزیه و تحلیل طیف فرکانس گسترده تر برانگیخته می شود. در نهایت، برداشت کننده های انرژی پیشنهادی، نمونه های کنسولی از سه ماده پایه مختلف بر اساس حداکثر ولتاژ و حداکثر خروجی توان لحظه ای آنها به صورت تجربی برای تحریک ضربه ای داده شده رتبه بندی می شوند. از سه ماده پایه در نظر گرفته شده، برداشت کننده های انرژی مبتنی بر فولاد و مس، حداکثر ولتاژ خروجی به ترتیب  $0.16 \text{ mV}$  و  $0.13 \text{ mV}$  تولید کردند که به ترتیب مربوط به حداکثر توان خروجی لحظه ای تقریباً  $1.96 \text{ nW}$  و  $1.69 \text{ nW}$  است. برداشت کننده انرژی مبتنی بر آلومینیوم در بین سه دستگاهی که در تولید  $0.81$  نانوات مشارکت داشتند، کمترین عملکرد را داشت.

---